Research Article

Yu-Wei Lu, Wen-Jie Zhou, Yongyao Li, Runhua Li, Jing-Feng Liu*, Lin Wu* and Haishu Tan*

Unveiling atom-photon quasi-bound states in hybrid plasmonic-photonic cavity

Abstract: Dissipation, often associated with plasmons, leads to decoherence and is generally considered fatal for quantum nonlinearities and entanglement. Counterintuitively, by introducing a dissipative plasmonic nanoantenna into a typical cavity quantum electrodynamics (QED) system, we unveil the wide existence of the atom-photon quasi-bound state (qBS), a kind of exotic eigenstate with anomalously small decay, in the hybrid plasmonic-photonic cavity. To derive the analytical condition of atom-photon qBS, we formulate a quantized two-mode model of the local density of states by connecting the interacting uncoupled cavity modes to the macroscopic QED. With resonant plasmon-photon coupling, we showcase the single-atom qBS that improves the efficiency of single-photon generation over one order of magnitude; and the two-atom qBS that significantly enhances spontaneous entanglement generation compared with a bare photonic cavity.

Notably, such single-atom and multi-atom qBS can be simultaneously accessed in realistic plasmonic-photonic cavities, providing a versatile platform for advanced quantum technologies, such as quantum light sources, quantum computation, and quantum information.

1 Introduction

With suppressed radiative leakage, single photons in a high-Q dielectric microcavity have the opportunity to interact repeatedly with a quantum emitter (QE), resulting in an enhanced coherent light–matter interaction and a strong coupling. Such strongly coupled microcavity-QE systems allow the on-chip manipulation, transmission, and storage of quantum states with high fidelity [1, 2]. However, their large physical volume (with at least one dimension on the order of the resonant wavelength) limits the further enhancement of the light–matter interaction in the traditional dielectric microcavity. Recently, the hybrid plasmonic-photonic cavity has emerged as a novel nanophotonic platform that can simultaneously exploit the advantages of both the low-loss microcavity and the large local field enhancement of plasmonic antenna [3–5]. In particular, when the microcavity is significantly red-detuned from the plasmonic antenna, the local density of states (LDOS), a fundamental quantity that governs the QE dynamics, manifests several-fold enhancement while the linewidth remains comparable to a bare microcavity [3, 4, 6–8]. This feature simultaneously enables high cooperativity of light–matter interaction and avoids undesirable dissipative losses. Accordingly, the red-detuned plasmonic-photonic cavity benefits various classical and quantum-optics applications, including biosensing [9, 10], nanolasers [11], optomechanics [12], strong light–matter interaction [13–15], and quantum light sources [16]. On the contrary, for the resonant plasmonic-photonic cavity (which is commonly characterized by much better field enhancements, mode volumes, and cooperativity), the LDOS is, however, strongly suppressed and dominated by the intrinsic ohmic loss of the plasmonic antenna,

*Corresponding authors: Jing-Feng Liu, College of Electronic Engineering, South China Agricultural University, Guangzhou 510642, China, E-mail: liujingfeng@scau.edu.cn; Lin Wu, Science, Mathematics and Technology (SMT), Singapore University of Technology and Design (SUTD), 8 Somapah Road 487372, Singapore, Singapore; and Institute of High Performance Computing, Agency for Science, Technology, and Research (A*STAR), 1 Fusionopolis Way, #16-16 Connexis 138632, Singapore, Singapore,
E-mail: lin_wu@sutd.edu.sg. https://orcid.org/0000-0002-3188-0640; and Haishu Tan, School of Physics and Optoelectronic Engineering, Foshan University, Foshan 528000, China,
E-mail: tanhaishu@fosu.edu.cn
Yu-Wei Lu, School of Physics and Optoelectronic Engineering, Foshan University, Foshan 528000, China. https://orcid.org/0000-0002-3174-6812
Wen-Jie Zhou, Science, Mathematics and Technology (SMT), Singapore University of Technology and Design (SUTD), 8 Somapah Road 487372, Singapore, Singapore
Yongyao Li, School of Physics and Optoelectronic Engineering, Foshan University, Foshan 528000, China; and Guangdong-Hong Kong-Macao Joint Laboratory for Intelligent Micro-Nano Optoelectronic Technology, Foshan University, Foshan 528000, China
Runhua Li, School of Physics and Optoelectronics, South China University of Technology, Guangzhou 510641, China

implying the weak coherent light–matter interaction in the near-resonance region.

Despite the inevitable large nonradiative dissipation in the resonant plasmon-photon coupling, in this work, we will show that introducing a resonant plasmonic antenna allows for forming an exotic eigenstate whose decay is equal to or even smaller than the original cavity quantum electrodynamics (QED) system. The underlying physical mechanism of this anomalously small decay is analogous to the accidental bound state in the continuum (BIC), which is a localized resonance with an infinite lifetime inside the continuum achieved through parameter tuning [17]. BIC was originally proposed in quantum mechanics when studying the one-dimensional Schrödinger equation [18] and the interference of two resonances associated with different channels [19], but it also flourished in many fields of physics, including the metamaterial and quantum material [20, 21], quantum optics [22–25], and acoustic systems [26, 27]. Particularly, in recent years, BIC has arisen as a new strategy to trap and guide the optical waves in various photonic systems [28–33]. Beyond these classical scattering and absorption phenomena, the quantum effects in BIC quantum systems play an important role in various quantum applications, such as the manipulation of quantum light [21, 24, 25] and the long-distance photon propagation and quantum entanglement in waveguide-QED systems [34–36]. In this work, based on the plasmonic-photonic cavity, we reveal the existence of quasi-bound states (qBS) for the atom–photon interaction. As illustrated in Figure 1a, the broadband plasmon resonance from the plasmonic antenna acts as the continuum in the plasmonic-photonic QED system. The atom–photon qBS appears due to the destructive interference of the "direct" and "plasmon-mediated" couplings between the microcavity and the QE. The resultant eigenenergy spectrum has triplet eigenenergy levels at the one-excitation subspace. The decay of lower and upper bands is about the quart linewidth of plasmon resonance, while the middle one with anomalously small decay defines the atom-photon qBS.

Obtaining the concrete condition of atom-photon qBS requires identifying different coupling pathways. However, the quantized treatment of the plasmonic-photonic cavity is complicated due to the dispersive and absorbing characteristics of materials, and the mutual coupling of two components. Two powerful and efficient methods, the quasinormal mode [8, 37] and the quantized pseudomode [3, 7, 38], have been applied to study the classical and quantum properties of the plasmonic-photonic cavity. Inspired by them and to elucidate the role of different coupling channels in forming the atom-photon qBS and determine the critical system parameters, we develop a simple and intuitive two-mode quantization model for the LDOS of the plasmonic-photonic cavity, where the mode parameters and the coupling rates with QE are obtained from bare components, leaving only the mode coupling determined by the simple curve fitting. We further demonstrate that the small decay of atom-photon qBS makes the plasmonic-photonic cavity advantageous in enhancing single-photon generation and the spontaneous entanglement generation (SEG) in the regime of on- and near-resonance plasmon-photon coupling.

2 Results and discussion

2.1 Two-mode model for LDOS of hybrid cavity

We consider a dipolar plasmonic antenna, where the higher-order modes are well separated from the dipolar plasmonic mode, then the hybrid plasmonic-photonic cavity can be treated as two coupled Lorentzian cavities. The full Hamiltonian of a two-level QE interacting with hybrid cavity reads $H = H_0 + H_I$, including the free Hamiltonian $H_0 = (\omega_0 - i\gamma/2)\,\sigma_+\sigma_- + (\omega_a - i\kappa_a/2)\,a^\dagger a + (\omega_c - i\kappa_c/2)\,c^\dagger c$ and the interaction Hamiltonian $H_I = g_a\left(a^\dagger\sigma_- + \sigma_+ a\right) + g_c\left(c^\dagger\sigma_- + \sigma_+ c\right) - g_1\left(a^\dagger c + c^\dagger a\right)$, where the decay of each component is introduced via quantum-jump approach and well approximately by the jump-free part [39], since we consider the single and weak excitation in this work. Here, a (or $a^\dagger$) and c (or $c^\dagger$) represent the bosonic annihilation (or creation) operators for the dipolar plasmonic mode and the microcavity mode, with resonance frequencies ω_a and ω_c, and decays κ_a and κ_c, respectively; $\sigma_- = |g\rangle\langle e|$ (or $\sigma_+ = |e\rangle\langle g|$) denotes the lowing (or raising) operator of QE with ω_0 and γ the corresponding transition frequency and decay of QE; g_a, g_c and g_1 are the coupling rates for QE-plasmon, QE-photon and plasmon-photon interaction, respectively. The spectral density of the hybrid cavity is expressed as: $J(\omega) = \int_{-\infty}^{+\infty} d\tau \Lambda(\tau) e^{i\omega t}$, with $\Lambda(\tau) = \left\langle \left[g_a a(\tau) + g_c c(\tau)\right]\left[g_a a^\dagger(0) + g_c c^\dagger(0)\right]\right\rangle$ [40, 41], which can be analytically obtained by calculating the environmental correlation functions from full Hamiltonian H, and separated into three parts (see details in Supporting Information S1):

$$J(\omega) = Re\left[J_a(\omega) + J_c(\omega) + J_{ac}(\omega)\right], \tag{1}$$
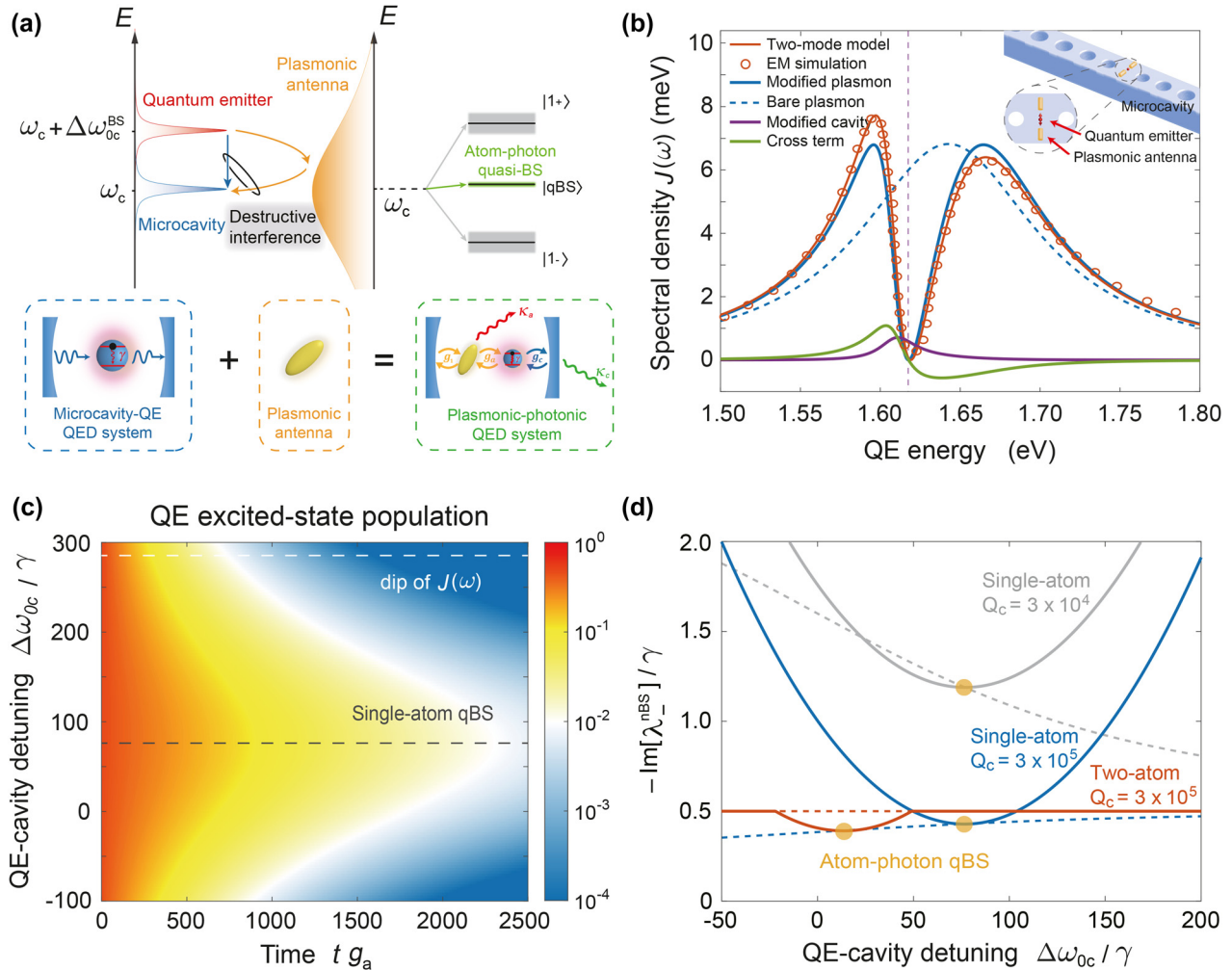
Figure 1: Atom-photon qBS in a hybrid plasmonic-photonic cavity QED system.
(a) Concept diagram of atom-photon qBS in hybrid cavity. The atom-photon qBS occurs due to the destructive interference between two coupling channels belonging to QE and photonic microcavity, which do not need to overlap. The resultant eigenenergy spectrum at the single-excitation subspace has triplet sublevels. (b) Application of the two-mode model to calculate the spectral density $J(\omega)$ and identify different components in a sample hybrid cavity QED system [4], where a QE with dipole moment $\mu = 60$ D at the gap center of a plasmonic antenna is placed on top of a dielectric nanobeam (inset). The vertical dashed line indicates the bare cavity resonance ω_c with decay rate $\kappa_c = 5.4$ μeV. (c) Relaxation dynamics of an initially excited QE (i.e., the color-map represents the excited-state population $\langle \sigma_+\sigma_- \rangle$ of QE) in the hybrid cavity as the function of QE-cavity detuning $\Delta\omega_{0c}$, with QE's decay rate $\gamma = 10$ μeV. The white and gray dashed lines indicate the dip of $J(\omega)$ and the optimal $\Delta\omega_{0c}$ corresponding to single-atom qBS, respectively. (d) The imaginary part of the calculated eigenenergy corresponding to atom-photon qBS as a function of the $\Delta\omega_{0c}$ for single-atom and two-atom cases at the different microcavity quality factors Q_c, while those of bare microcavity are also shown for comparison (dashed lines with the same color). The yellow dots label the conditions of the atom-photon qBS.

with

$$J_X(\omega) = ig_X^2 \chi_X(\omega) \left[1 - g_1^2 \chi_a(\omega)\chi_c(\omega)\right]^{-1}, \qquad (2)$$

$$J_{ac}(\omega) = i2g_a g_c g_1 \chi_a(\omega)\chi_c(\omega) \left[1 - g_1^2 \chi_a(\omega)\chi_c(\omega)\right]^{-1}, \quad (3)$$

where $\chi_X(\omega) = [(\omega - \omega_X) + i\kappa_X/2]^{-1}$ for $X = a, c$ is the polarizability of bare components. $J_a(\omega)$ and $J_c(\omega)$ represent the modified plasmon and cavity response,

respectively, and $J_{ac}(\omega)$ is the crossing interference term. Therefore, $J(\omega)$ can be generated via the parameters of bare cavity modes and their coupling rate. The normalized LDOS, i.e., Purcell factor, is related to the spectral density through the relationship $P(\omega) = J(\omega)/J_0(\omega)$, where $J_0(\omega) = \omega^3\mu^2/6\pi^2\hbar\varepsilon_0 c^3$ is the spectral density in free space (ε_0 the vacuum permittivity and c the speed of light) for a QE with dipole moment μ.

To validate our model, we take a recently reported hybrid cavity [4] as an example, i.e. a gold dimer on nanobeam cavity shown as the inset of Figure 1b, and parametrize its spectral density. For a QE with $\mu = 60$ D, we obtain the parameters $(\omega_a, \kappa_a, g_a) = (1.643$ eV, 0.136 eV, 21 meV) for the bare plasmonic antenna and $(\omega_c, \kappa_c, g_c) = (1.618$ eV, 5.4 μeV, 0.94 meV) for the bare nanobeam microcavity (with quality factor $Q_c \equiv \omega_c/\kappa_c = 3 \times 10^5$). Such hybrid cavity can be considered as resonant coupling since the plasmon–photon detuning $\Delta\omega_{ac} = \omega_a - \omega_c \approx 0.18\kappa_a$. Subsequently, the mode coupling g_1 can be evaluated by a simple curve fitting using Eqs (1)–(3), and the optimal value is found to be $g_1 = 32$ meV. The corresponding LDOS generated by our two-mode model is plotted in Figure 1b, which matches well with the classical electromagnetic (EM) simulation. More essentially, our model breaks down the spectral density into three terms that correspond to different coupling pathways. As shown in Figure 1b, the contribution of the plasmon-modified cavity response (purple) can be neglected compared to the cavity-modified plasmon response (blue), which dominates the spectral density. Around the cavity resonance $\omega_c = 1.618$ eV, the interference cross term (green) changes its sign and leads to an asymmetric spectral density. Meanwhile, the cavity-modified plasmon response (blue), and hence the spectral density (red), are strongly suppressed, where a dip can be clearly observed due to the destructive interference between the nanobeam cavity and the plasmonic antenna. This leads to the slower relaxation (longer lifetime) of an excited QE with transition frequency lying in this region when the QE-cavity detuning $\Delta\omega_{0c} = \omega_0 - \omega_c$ is close to zero, as detailed in Figure 1c where we normalize $\Delta\omega_{0c}$ to the decay rate $\gamma = 10$ μeV of QE. The slowest relaxation occurs when QE is slightly blue-detuned (~0.76 meV) from the nanobeam cavity, neither on resonance nor at the dip of $J(\omega)$ but between them. This slowest relaxation condition, relevant to the atom-photon quasi-bound states (e.g., single-atom qBS in this case), will be explained in more detail in the following. It should be emphasized that the microcavity resonance frequency $\omega_c = 1.618$ eV and the QE's decay rate $\gamma = 10$ μeV are kept constant throughout this work as the reference values.

2.2 Generalized analytical condition of N-atom-photon qBS

Based on our quantized two-mode model, we can unravel the underlying mechanism and generalize the plasmonic-photonic QED system to the N-atom case. The dynamics of

the plasmonic-photonic QED system follows the quantum master equation (QME):

$$\frac{\partial\rho}{\partial t} = i[\rho, H_M] + \frac{\kappa_a}{2}\mathcal{L}_a(\rho) + \frac{\kappa_c}{2}\mathcal{L}_c(\rho) + \sum_i \frac{\gamma}{2}\mathcal{L}_{\sigma_-^{(i)}}(\rho), \quad (4)$$

where $\mathcal{L}_{\hat{o}}(\rho) = 2\hat{o}\rho\hat{o}^\dagger - \hat{o}^\dagger\hat{o}\rho - \rho\hat{o}^\dagger\hat{o}$ is the Liouvillian superoperator with $\hat{o}$ being an operator. The corresponding multi-QE Hamiltonian H_M reads:

$$H_M = \omega_a a^\dagger a + \omega_c c^\dagger c + \sum_i \omega_0 \sigma_+^{(i)}\sigma_-^{(i)}$$
$$+ \sum_i g_a^{(i)}\left(a^\dagger\sigma_-^{(i)} + \sigma_+^{(i)}a\right)$$
$$+ \sum_i g_c\left(c^\dagger\sigma_-^{(i)} + \sigma_+^{(i)}c\right), \quad (5)$$

where we have made the assumption of identical QEs having different coupling strengths with the plasmonic antenna, considering that the EM field distribution of plasmonic mode can drastically vary within a few nanometers from the antenna. In the case of single excitation or the system is driven by a weak coherent field, the system dynamics can be well described by the jump-free part of $\mathcal{L}_{\hat{o}}(\rho)$. We can derive a non-Hermitian Hamiltonian $H' = H'_0 + H'_I$ from the above QME, with the free Hamiltonian $H'_0 = \sum_i (\omega_0 - i\gamma/2)\sigma_+^{(i)}\sigma_-^{(i)} + (\omega_a - i\kappa_a/2)a^\dagger a + (\omega_c - i\kappa_c/2)c^\dagger c$ and the interaction Hamiltonian $H'_I = \sum_i g_a^{(i)}\left(a^\dagger\sigma_-^{(i)} + \sigma_+^{(i)}a\right) + \sum_i g_c\left(c^\dagger\sigma_-^{(i)} + \sigma_+^{(i)}c\right) - g_1(a^\dagger c + c^\dagger a)$. Rewriting the Hamiltonian H' in the one-excitation subspace in matrix form (see details in Supporting Information S2), in the limit of $\kappa_a \gg \kappa_c, \gamma$, which is realistic for plasmonic-photonic cavity, we find the solution for a purely real eigenenergy if the QE-cavity detuning $\Delta\omega_{0c}$ meets the following requirement:

$$\Delta\omega_{0c}^{nBS} = g_c\left(\frac{Ng_1}{\sum_i g_a^{(i)}} - \frac{\sum_i g_a^{(i)}}{g_1}\right). \quad (6)$$

At this point, one of eigenenergies is purely real, which is $\lambda_-^{nBS} = \omega_c + Ng_1g_c/\sum_i g_a^{(i)}$, with N being the number of QEs. For single-atom case with $N = 1$, the above condition is $\Delta\omega_{0c}^{BS} = g_c(g_1/g_a - g_a/g_1)$, which takes the same form as the condition of Friedrich-Wintgen BIC [17, 19], and thus we call this eigenstate as the single-atom-photon qBS. Note that the genuine bound state can hardly form due to the existence of decays κ_c and γ. In Figure 1c, this single-atom qBS is indicated by a dashed gray line, which coincides with the slowest relaxation of QE.

To make things more general, we plot the eigenenergy corresponding to the single-atom and two-atom qBS as a function of QE-cavity detuning $\Delta\omega_{0c}$ in Figure 1d, where the imaginary part of eigenenergy (i.e., decay) reaches the minimum (highlighted using yellow dots) at the qBS condition given by Eq. (6) in both cases. For the single-atom case, it is evident that the decay of single-atom qBS (solid lines) is generally smaller than that of the atom-like branch of bare microcavity (dashed lines) at the qBS condition. Even if the qBS condition is not exactly fulfilled, this anomalously small decay can persist over a finite frequency range around $\Delta\omega_{0c}^{nBS}$ (gray lines). However, it is harder to recognize this feature for a high-Q cavity (blue lines). For the two-atom case (orange lines), the decay at qBS is smaller than that of the two-atom dark state in a bare microcavity (i.e., $\gamma/2$), while it recovers back to $\gamma/2$ when far from the qBS condition. In short, it is instructive to derive the generalized analytical condition of N-atom-photon qBS using Eq. (6) for any practical application, and we will show its applicability to predict the optimal conditions for quantum-optics applications in the latter part of the work.

2.3 Quantum-optics applications of atom-photon qBS

The feature of small decay makes atom-photon qBS beneficial for many quantum-optics applications. Here, we will showcase two examples: single-atom qBS for improving the efficiency of single-photon generation using conventional photon blockade (CPB) and two-atom qBS for enhancing the spontaneous entanglement generation (SEG) between two QEs.

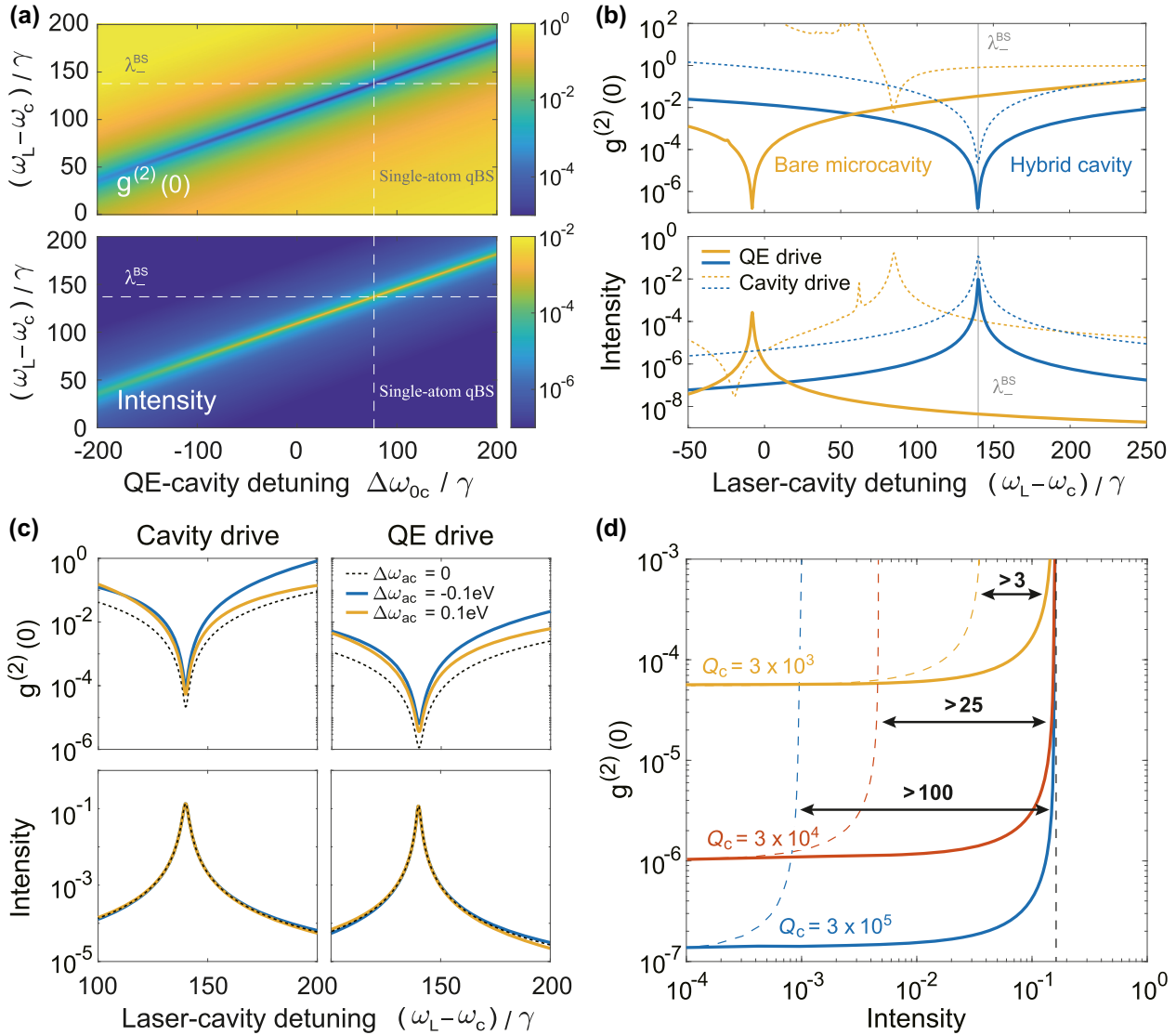### 2.3.1 Single-atom qBS for single-photon generation

Single-photon generation via conventional photon blockade (CPB) utilizes the anharmonic energy levels to block the absorption of the second photon. The zero-time-delay correlation function $g^{(2)}(0) < 1$, i.e., photon antibunching, signs the occurrence of single-photon blockade. As it takes place when the system is driven at the frequency of one of the eigenstates at the single-excitation subspace [42], the feature of small decay makes single-atom qBS particularly beneficial for improving the photon intensity, and hence the efficiency of single-photon generation using CPB. To investigate the performance of single-photon generation, a weak coherent field is applied to the system by implementing a driving Hamiltonian H_{drive} in QME in Eq. (4),

which takes the form of $H_{\text{drive}} = \Omega\left(e^{-i\omega_L t}\sigma_+ + \sigma_- e^{i\omega_L t}\right)$ for QE drive and $H_{\text{drive}} = \Omega\left(e^{-i\omega_L t}c^\dagger + ce^{i\omega_L t}\right)$ for cavity drive, where Ω and ω_L are the intensity and the laser frequency of driving field, respectively. The numerical calculation details for the single-photon intensity $\left(I_c = \langle c^\dagger c\rangle\right)$ and the purity $(g^{(2)}(0) = \langle c^\dagger c^\dagger cc\rangle/I_c^2)$ can be found in Supporting Information S3.

Figure 2a shows the calculated zero-time-delay correlation function $g^{(2)}(0)$ and single-photon intensity I_c of the nanobeam microcavity for the cavity-driven case by varying pump frequency ω_L and QE-cavity detuning $\Delta\omega_{0c}$. We can see that the best single-photon purity and highest intensity are simultaneously achieved at single-atom qBS. We then compare the single-photon performance of hybrid cavity with single-atom qBS and bare nanobeam microcavity in Figure 2b. It shows that when achieving the same single-photon purity, $g^{(2)}(0) = 10^{-7}$ with QE drive, the intensity of hybrid cavity (solid blue line) is boosted more than 36-fold compared to a bare nanobeam microcavity (orange solid line). While driving the cavity with a stronger pump (dashed lines), the single-photon purity $g^{(2)}(0)$ can be improved over two orders of magnitude when achieving similar intensity.

On the other hand, it is worth noting that though the resonant plasmon-photon coupling manifests the best single-photon performance, the moderate plasmon-photon detuning does not significantly degrade the single-photon purity and intensity. As indicated in Figure 2c, the increase of minimum $g^{(2)}(0)$ is within one order of magnitude with plasmon-photon detuning $\Delta\omega_{ac} = \omega_a - \omega_c = \pm 0.1$ eV, compared to the resonant case; whereas the variation of intensity is negligible. Furthermore, we evaluate from Figure 2a that both the intensity and purity decrease less than 10% with QE-microcavity detuning $\left|\Delta\omega_{0c} - \Delta\omega_{0c}^{nBS}\right| < 10\gamma$. Therefore, the single-atom qBS indeed makes the plasmonic-photonic cavity as a robust platform for high-efficiency single-photon source.

We further compare the intensity-purity curves for hybrid cavity and bare microcavity, obtained by increasing the driving strength for different microcavity quality factor Q_c under QE drive condition, as illustrated in Figure 2d. There is clearly an upper bound for the intensity, which is independent of Q_c (but mainly limited by QE-photon coupling rate g_c). A high Q_c improves the single-photon purity with significantly smaller $g^{(2)}(0)$. Compared to a bare microcavity (dashed lines) achieving the same $g^{(2)}(0)$ in the weak pump limit $\left(Q_c = 3 \times 10^5\right)$, the hybrid cavity (solid lines) demonstrates a hundredfold enhancement of the maximum intensity. Such enhancement drops from 100 to 25 as Q_c decreases from 3×10^5 to 3×10^4. These results

Figure 2: Single-atom qBS for single-photon generation.
(a) The zero-time-delay correlation function $g^{(2)}(0)$ (upper panel) and intensity (lower panel) in the cavity-driven case as the function of QE-cavity detuning $\Delta\omega_{0c}$ and the laser-cavity detuning, with ω_L the laser frequency. The vertical and horizontal dashed lines correspond to the optimal $\Delta\omega_{0c}$ and the eigenenergy of single-atom qBS, respectively. (b) The $g^{(2)}(0)$ (upper panel) and intensity (lower panel) versus laser-cavity detuning for bare microcavity (yellow lines) and hybrid cavity (blue lines) with single-atom qBS for QE drive (solid lines) and cavity drive (dashed lines). The light gray lines indicate the location of λ_-^{BS}. The driving strength is $\Omega = 0.1\gamma$ for QE drive, and $\Omega = \gamma$ for cavity drive. (c) The $g^{(2)}(0)$ (upper panel) and intensity (lower panel) versus laser-cavity detuning for hybrid cavity with three different plasmon-photon detuning $\Delta\omega_{ac}$. The driving strength is $\Omega = \gamma$. (d) The intensity-purity curves for the hybrid cavity (solid lines) and bare microcavity (dashed lines) with different quality factors under QE drive. Here, $\Delta\omega_{0c} = \Delta\omega_{0c}^{BS}$ for hybrid cavity, while $\Delta\omega_{0c}$ of bare microcavity are 1960γ, 1000γ, and 320γ for $Q_c = 3 \times 10^3$, $Q_c = 3 \times 10^4$ and $Q_c = 3 \times 10^5$, respectively. The vertical black dashed line indicates the achievable maximum intensity of hybrid cavity. Parameters of the hybrid cavity are kept the same as those in Figure 1 unless specially noted, where the microcavity resonance frequency $\omega_c = 1.618$ eV and the QE's decay rate $\gamma = 10$ μeV are kept constant throughout this work as the reference values.

suggest that the figure of merit of the microcavity is critical for the efficiency enhancement of single-photon blockade with single-atom qBS.

The single-photon generation discussed in this work is based on the conventional photon blockade (CPB) that

utilizes the anharmonicity of the discrete level structure. An alternative route to generate a single photon from coherent light is to induce the destructive interference between all possible transition pathways for the two-photon state of the microcavity, called unconventional photon blockade

(UPB) [42]. The intensity (efficiency) of UPB is generally lower than CPB by orders of magnitude (e.g., in a QE-microcavity system [43]) as CPB occurs at one of the peaks of intensity while UPB does not. For example, the intensity of UPB in a coupled quantum-dot-cavity system is 0.004 for $g^{(2)}(0) \approx 0.005$ [44], while the intensity of CPB in our system is roughly 0.2 for $g^{(2)}(0) = 0.001$ $(Q_c = 3 \times 10^3)$, as indicated in Figure 2d. The single-atom qBS combined with CPB is a promising scheme for building a high-efficiency quantum light source.

2.3.2 Two-atom qBS for spontaneous entanglement generation

The creation of entangled states between the qubits is a key task of quantum computation and quantum information processing [45]. The entanglement is commonly measured by the concurrence $C(t)$ [46], which in our system is given by the simple expression $C(t) = 2 \left| C_{eg}(t) C_{ge}^*(t) \right|$, with $C_{eg}(t)$ and $C_{ge}(t)$ the probability amplitudes of two single-excitation states that one QE is in the excited state while the other is in the ground state at any point of time. To calculate $C(t)$, we set one QE initially in the excited state and the other in the ground state and allow the two QEs to evolve spontaneously into an entangled state. During the evolution, we can identify the achievable maximal value of concurrence, i.e., max[$C(t)$]. The larger the value of max[$C(t)$], the better the entanglement between two QEs is. Here, we show that the two-atom qBS can enhance the spontaneous entanglement generation (SEG) between two QEs, where our generalized analysis of N-atom-photon qBS is applicable with $N = 2$.

We first study the impact of different QE-plasmon couplings $g_a^{(i)}$ (i represents different QEs) on the decay of two-atom qBS in Figure 3a and find that $g_a^{(1)} = g_a^{(2)}$ is the optimal condition for minimum decay, which is slightly smaller than $\gamma/2$ and approaches $\gamma/2$ as the coupling rate of QE-plasmon interaction increases. Therefore, we only consider the case of $g_a^{(1)} = g_a^{(2)}$ in the following discussions. We then plot the concurrence $C(t)$ of dynamical entanglement generation between an initially excited QE and a ground state QE as a function of the QE-cavity detuning in Figure 3b. Evidently, the $C(t)$ demonstrates oscillating patterns around the two-atom qBS, where the most persistent oscillation occurs exactly at the two-atom qBS (highlighted by the dashed line). Taking a closer look at the inset, the max[$C(t)$] of the hybrid cavity is ∼0.77, while those of the bare components are <0.48.

The oscillating behavior of $C(t)$ originates from the dissipative atom-photon interaction mediated by the

plasmonic antenna, but the damping of oscillation is determined by the decay of eigenenergies and thus related to the two-atom qBS. This can be better understood from an approximate analytical expression of $C(t)$ (see detailed derivation in Supporting Information S4):

$$C(t) \approx \frac{1}{2} \left| e^{-\gamma_- t} \frac{|\kappa - i\Delta\omega_{0c} + u|^2}{4|u|^2} - e^{-\gamma t} \right.$$
$$- i e^{-\frac{\gamma}{2}t} e^{-\frac{\gamma_-}{2}t} \left(\frac{\kappa Re[u]}{|u|^2} + 1 \right)$$
$$\left. \times \sin\left(\frac{\mathrm{Im}\left[u - 2\gamma_p\right] + \Delta\omega_{0c}}{2} t \right) \right|, \quad (7)$$

with $\gamma_- = \kappa + \gamma/2 - Re\left[u - 2\gamma_p\right]$, $u = \sqrt{-8g_{ca}g_{ac} + \left[-i\Delta\omega_{0c} + (\kappa - 2\gamma_p - \gamma/2)\right]^2}$, and $\kappa = \kappa_c/2 + \kappa_p$. Here, $\kappa_p = 2g_1^2/\kappa_a$ and $\gamma_p = 2g_a^2/(-i2\Delta\omega_{0c} + \kappa_a)$ are the plasmon-induced cavity and QE decays, respectively; $g_{ca} = g_c + i2g_ag_1/\kappa_a$ and $g_{ac} = g_c + i2g_ag_1/(-i2\Delta\omega_{0c} + \kappa_a)$ are the plasmon-mediated cavity-to-QE and QE-to-cavity couplings, respectively. Equation (7) is deduced from the effective Hamiltonian $H_{eff} = \sum_{i,j} \left[(\omega_c + \Delta\omega_{0c} - i\gamma/2)\delta_{ij} - i\gamma_p\right]\sigma_+^{(i)}\sigma_-^{(j)} + (\omega_c - i\kappa/2)c^\dagger c + \sum_i \left(g_{ac}c^\dagger\sigma_-^{(i)} + g_{ca}\sigma_+^{(i)}c\right)$, obtained by adiabatically eliminating the plasmon operators. It can be seen from the inset of Figure 3b that our analytical expression Eq. (7) accords quite well with the numerical solution. Upon further analysis of Eq. (7) for the resonant condition ($\Delta\omega_{0c} = 0$), the $C(t)$ oscillates due to Im$\left[u - 2\gamma_p\right] \neq 0$, which results from the co-existence of the coherent and the dissipative components in the effective atom-photon interaction for the case of hybrid cavity. Another point to note from Eq. (7), the parameter γ_- (corresponding to the damping of oscillations since $\gamma_- \gg \gamma$) plays an essential role in determining the longtime dynamics of concurrence. In Figure 4 of Supporting Information, we show that γ_- reaches the minimum at two-atom qBS. It explains why two-atom qBS corresponds to the most persistent oscillations of $C(t)$.

The competing coherent and dissipative interaction combined with two-atom qBS enables higher concurrence of SEG in the plasmonic-photonic cavity. Figure 3c and e) compare the maximum concurrence (max[$C(t)$]) of SEG in the hybrid cavity for resonant QE-cavity coupling condition and two-atom qBS condition, respectively, as the function of QE-photon coupling g_c and plasmon-photon coupling g_1. For the resonant case in Figure 3c, larger plasmon-photon coupling g_1 is beneficial for higher concurrence. On the other hand, there is an optimal g_1 for the case of two-atom qBS, see solid black line in Figure 3e. Clearly,
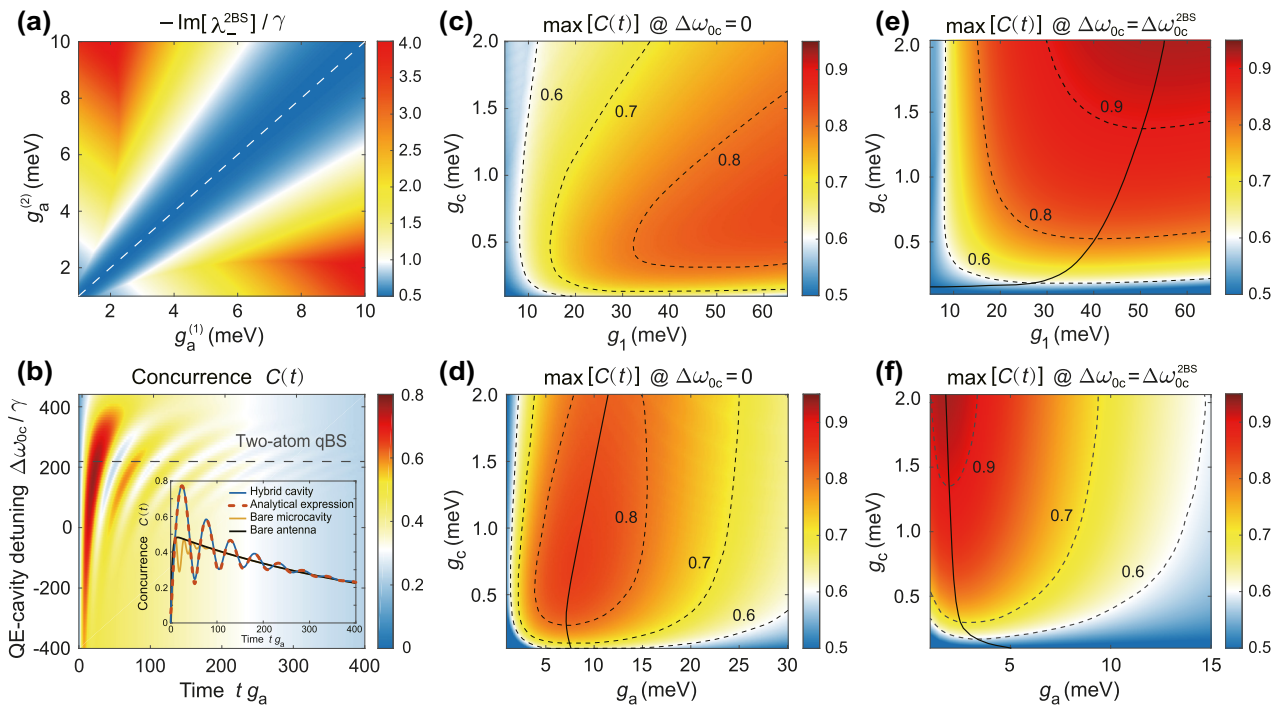
**Figure 3:** Two-atom qBS for spontaneous entanglement generation (SEG).
(a) The imaginary part of the eigenenergy of two-atom qBS as the function of QE-plasmon coupling rates $g_a^{(1)}$ and $g_a^{(2)}$, normalized by the constant QE's decay rate $\gamma = 10$ µeV. The white dashed line traces the minimum decay. (b) Concurrence of SEG as the function of $\Delta\omega_{0c}$. Inset: Comparison of the concurrence of hybrid cavity with an approximate analytical expression. Concurrence of bare microcavity and plasmonic antenna are also shown for comparison. (c) and (d) Maximum concurrence max[$C(t)$] as the function of QE-photon coupling rate g_c and plasmon-photon coupling rate g_1, QE-photon coupling rate g_c and QE-plasmon coupling rate g_a, respectively, in the condition of resonant coupling $\Delta\omega_{0c} = 0$. (e) and (f) are the same as (b) and (c) but for the case of two-atom qBS with $\Delta\omega_{0c} = \Delta\omega_{0c}^{2BS}$. The black solid lines trace the maximum concurrence with respect to the QE-photon coupling rate g_c. The parameters of the resonant plasmon-photon hybrid cavity are $\omega_a = \omega_c = 1.618$ eV, $g_a = 5$ meV, $g_c = 0.6$ meV, $g_1 = 20$ meV, $\kappa_a = 0.12$ eV and $\kappa_c = 0.5$ meV ($Q_c \sim 3000$). The numerical calculations of concurrence are performed using QuTip [47], with system's initial condition: one QE is in the excited state and the other is in the ground state, while the cavity fields are in the vacuum state.

the two-atom qBS condition improves the maximum concurrence from 0.84 to 0.95 and meanwhile lowers the requirement of g_1 for achieving the same concurrence. This advantage is more prominent with strong QE-photon coupling g_c. For example, with $g_c = 2$ meV, a moderate plasmon–photon coupling $g_1 = 20-40$ meV can increase the concurrence by ~30%. Similarly, Figure 3d and f illustrates the dependence of the concurrence on QE-photon coupling g_c and QE-plasmon coupling g_a. The optimal QE-plasmon coupling g_a to reach an even higher maximum concurrence at the two-atom qBS condition in Figure 3f is smaller than that for the resonant QE-cavity coupling condition in Figure 3d. These features will enhance the SEG and benefit the entanglement transport via microcavity.

To further understand the SEG in hybrid cavity, we calculate the fidelity $F_{\pm} = \langle\Psi_{\pm}|\rho|\Psi_{\pm}\rangle$ and show in Figure 5 of Supporting Information, with $|\Psi_+\rangle$ and $|\Psi_-\rangle$ being the even and odd Bell states, respectively. The

results indicate that the created entangled state is the odd Bell state, and max[F_-] $\approx$ max[$C(t)$] for high concurrence. Compared to the recently reported SEG scheme based on the chiral waveguide (max[F_-] = max[$C(t)$] = 0.92) [48], which is promising for constructing the quantum networks, our system can achieve a comparable concurrence and fidelity of 0.95. This value is also higher than SEG of both the individual plasmonic antenna (~0.87) [49] and the single-mode microcavity (~0.89) [50]. Furthermore, it is important to note that the underlying physical mechanism for our atom-photon qBS is fundamentally different from the dissipation-induced stationary entanglement [50], although the plasmonic antenna plays the role of dissipative environment (the continuum). While the dissipation-induced stationary entanglement is attributed to the anti-symmetric state of two QEs decoupled from the cavity due to the dipole–dipole interaction, our atom-photon qBS results from the destructive interference of
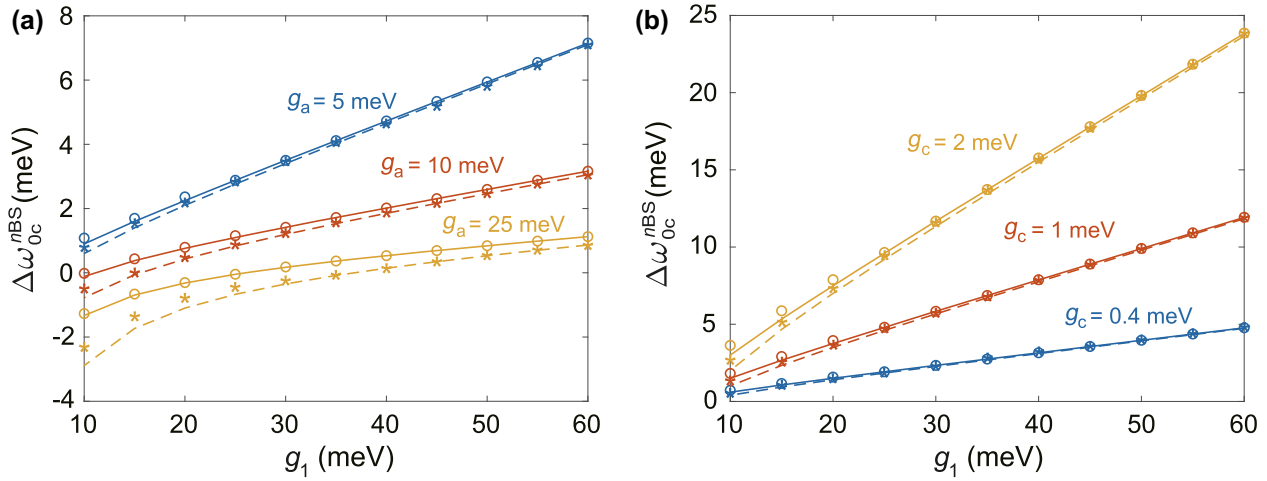
Figure 4: Applicability of analytical condition $\Delta\omega_{0c}^{nBS}$ to predict the optimal conditions for quantum-optics applications. Comparison of $\Delta\omega_{0c}^{BS}$ (solid lines) and the optimal QE-cavity detuning $\Delta\omega_{0c}$ corresponding to the single-photon blockade with highest efficiency (hollow circles), as well as $\Delta\omega_{0c}^{2BS}$ (dashed lines) and the optimal $\Delta\omega_{0c}$ for maximum concurrence in the longtime limit (stars) for different cases of **(a)** QE-plasmon coupling rate g_a and (b) QE-photon coupling rate g_c, as a function of plasmon-photon coupling rate g_1. All other parameters are kept the same as those in Figure 3 unless mentioned otherwise.

two coupling pathways. Still, placing the QEs inside the gap center of the plasmonic antenna and utilizing the dipole–dipole interaction makes it possible to realize the stationary entanglement in our setup.

2.3.3 Applicability of analytical condition $\Delta\omega_{0c}^{nBS}$

Up to this point, we have demonstrated two quantum optics applications of qBS and provided a handy formula for the condition of atom-photon qBS $\Delta\omega_{0c}^{nBS}$ in Eq. (6) to guide the design of experiment. However, we have neglected the decays (κ_c and γ) in deriving our analytical condition Eq. (6), which may influence its applicability. Next in Figure 4, we will investigate the robustness of $\Delta\omega_{0c}^{nBS}$ to accurately predict the optimal condition for single-photon blockade and SEG, by comparing it with the optimal $\Delta\omega_{0c}$ (hollow circles for single-photon blockade and stars for SEG) obtained using various coupling parameters and taking into account the noise values $\gamma = 10\,\mu\text{eV}$, $\kappa_a = 0.12\,\text{eV}$, and $\kappa_c = 0.5\,\text{meV}$. We can see that $\Delta\omega_{0c}^{nBS}$ generally shows good agreement for larger plasmon-photon coupling g_1, smaller QE-plasmon coupling g_a and QE-photon coupling g_c; but $\Delta\omega_{0c}^{2BS}$ (dashed lines) is less accurate for larger g_a and g_c at smaller g_1. Furthermore, $\Delta\omega_{0c}^{2BS}$ is close to $\Delta\omega_{0c}^{BS}$ for small g_a and g_c, and approaches $\Delta\omega_{0c}^{BS}$ as g_1 increases, especially for the case of $g_a = 5$ meV and $g_c = 0.4$ meV as indicated in Figure 4a and b), where we can see that $\Delta\omega_{0c}^{2BS} \approx \Delta\omega_{0c}^{BS}$ for $g_1 > 30$ meV. This suggests that it is possible to simultaneously access the single- and multi-atom qBS, and such hybrid cavities with the

desirable level of plasmon-photon coupling have already been reported [4, 7]. In summary, the hybrid cavity can indeed be a versatile platform for diverse quantum-optics applications.

3 Conclusion and outlooks

With a quantized two-mode model for the LDOS of the plasmonic–photonic hybrid cavity, we unveil the formation of the atom-photon qBS due to the interference of different coupling pathways between QE and microcavity. Such dissipation-mediated light–matter interaction allows migrating the notion of Friedrich–Wintgen BIC into the plasmonic-photonic QED systems, leading to anomalously small decay for one of their eigenstates. Based on its small eigenenergy decay, we demonstrate two quantum-optics applications of atom-photon qBS with improved performance. Evidently, atom-photon qBS shows significant advantages in achieving high-efficiency single-photon generation and enhancing spontaneous entanglement generation. We also provide a generalized analytical condition of N-atom-photon qBS with N the number of QEs involved to help the future design of the experiments. To a larger extent, our work demonstrates a novel quantum-optics phenomenon in the hybrid cavity, which holds great potential for integrated optics, quantum optics, and quantum information applications. Nevertheless, it is worth noting that we consider the cryogenic temperature in this work, excluding the effect of pure dephasing.

A brief discussion on the impact of pure dephasing on single-photon generation and spontaneous entanglement generation can be found in Supporting Information S5. Moving forward, we could extend the work by including more complex quantum effects, such as the synthetic magnetic flux [51, 52] and the environment-mediated Fano effect [53], and investigate more practical hybrid systems, for instance, those based on Mie nanoresonators [54, 55], and the strong coupling between plasmon and 2D transition metal dichalcogenide materials [56].

References

[1] J. M. Raimond, M. Brune, and S. Haroche, "Manipulating quantum entanglement with atoms and photons in a cavity," *Rev. Mod. Phys.*, vol. 73, pp. 565−582, 2001.

[2] I. Georgescu and F. Nori, "Quantum technologies: an old new story," *Phys. World*, vol. 12, pp. 16−17, 2012.

[3] H. M. Doeleman, E. Verhagen, and A. F. Koenderink, "Antenna−cavity hybrids: matching polar opposites for purcell enhancements at any linewidth," *ACS Photonics*, vol. 3, pp. 1943−1951, 2016.

[4] M. Kamandar Dezfouli, R. Gordon, and S. Hughes, "Modal theory of modified spontaneous emission of a quantum emitter in a hybrid plasmonic photonic-crystal cavity system," *Phys. Rev. A*, vol. 95, p. 013846, 2017.

[5] H. Zhang, Y. C. Liu, C. Wang, N. Zhang, and C. Lu, "Hybrid photonic-plasmonic nanocavity with ultra-high Q/V," *Opt. Lett.*, vol. 45, pp. 4794−4797, 2020.

[6] H. M. Doeleman, C. D. Dieleman, C. Mennes, B. Ehrler, and A. F. Koenderink, "Observation of cooperative purcell enhancements in antenna−cavity hybrids," *ACS Nano*, vol. 14, pp. 12027−12036, 2020.

[7] I. Medina, F. J. García-Vidal, A. I. Fernández-Domínguez, and J. Feist, "Few-mode field quantization of arbitrary electromagnetic spectral densities," *Phys. Rev. Lett.*, vol. 126, p. 093601, 2021.

[8] S. Franke, S. Hughes, M. K. Dezfouli, et al., "Quantization of quasinormal modes for open cavities and plasmonic cavity quantum electrodynamics," *Phys. Rev. Lett.*, vol. 122, p. 213901, 2019.

[9] V. R. Dantham, S. Holler, C. Barbre, et al., "Label-free detection of single protein using a nanoplasmonic-photonic hybrid microcavity," *Nano Lett.*, vol. 13, pp. 3347−3351, 2013.

[10] F. Liang, Y. Guo, S. Hou, and Q. Quan, "Photonic-plasmonic hybrid single-molecule nanosensor measures the effect of fluorescent labels on DNA-protein dynamics," *Sci. Adv.*, vol. 3, p. e1602991, 2017.

[11] T. Zhang, S. Callard, C. Jamois, et al., "Plasmonic-photonic crystal coupled nanolaser," *Nanotechnology*, vol. 25, p. 315201, 2014.

[12] M. K. Dezfouli, R. Gordon, and S. Hughes, "Molecular optomechanics in the anharmonic cavity-QED regime using hybrid metal−dielectric cavity modes," *ACS Photonics*, vol. 6, pp. 1400−1408, 2019.

[13] J. N. Liu, Q. Huang, K. K. Liu, S. Singamaneni, and B. T. Cunningham, "Nanoantenna−microcavity hybrids with highly cooperative plasmonic−photonic coupling," *Nano Lett.*, vol. 17, pp. 7569−7577, 2017.

[14] P. Peng, Y. C. Liu, D. Xu, et al., "Enhancing coherent light-matter interactions through microcavity-engineered plasmonic resonances," *Phys. Rev. Lett.*, vol. 119, p. 233901, 2017.

[15] Y. F. Xiao, Y. C. Liu, B. B. Li, et al., "Strongly enhanced light-matter interaction in a hybrid photonic-plasmonic resonator," *Phys. Rev. A*, vol. 85, p. 031805, 2012.

[16] K. G. Cognée, H. M. Doeleman, P. Lalanne, and A. F. Koenderink, "Cooperative interactions between nano-antennas in a high-Q cavity for unidirectional light sources," *Light Sci. Appl.*, vol. 8, p. 115, 2019.

[17] C. W. Hsu, B. Zhen, A. D. Stone, J. D. Joannopoulos, and M. Soljačić, "Bound states in the continuum," *Nat. Rev. Mater.*, vol. 1, p. 16048, 2016.

[18] J. von Neuman and E. Wigner, "Uber merkwürdige diskrete Eigenwerte. Uber das Verhalten von Eigenwerten bei adiabatischen prozessen," *Phys. Z.*, vol. 30, p. 467, 1929.

[19] H. Friedrich and D. Wintgen, "Interfering resonances and bound states in the continuum," *Phys. Rev. A*, vol. 32, pp. 3231−3242, 1985.

[20] Q. Zhou, Y. Fu, L. Huang, et al., "Geometry symmetry-free and higher-order optical bound states in the continuum," *Nat. Commun.*, vol. 12, p. 4390, 2021.

[21] Q. Y. Liang, A. V. Venkatramani, S. H. Cantu, et al., "Observation of three-photon bound states in a quantum nonlinear medium," *Science*, vol. 359, pp. 783−786, 2018.

[22] K. Koshelev, A. Bogdanov, and Y. Kivshar, "Meta-optics and bound states in the continuum," *Sci. Bull.*, vol. 64, pp. 836−842, 2019.

[23] Y. W. Lu, J. F. Liu, Z. Liao, and X. H. Wang, "Plasmonic-photonic cavity for high efficiency single-photon blockade," *Sci. China Phys. Mech. Astron.*, vol. 64, p. 274212, 2021.

[24] M. Ahumada, P. A. Orellana, and J. C. Retamal, "Bound states in the continuum in whispering gallery resonators," *Phys. Rev. A*, vol. 98, p. 023827, 2018.

[25] M. Cotrufo and A. Alù, "Excitation of single-photon embedded eigenstates in coupled cavity−atom systems," *Optica*, vol. 6, p. 799, 2019.

[26] A. A. Maznev and A. G. Every, "Bound acoustic modes in the radiation continuum in isotropic layered systems without periodic structures," *Phys. Rev. B*, vol. 97, p. 014108, 2018.

[27] O. Haq and S. Shabanov, "Bound states in the continuum in elasticity," *Wave Motion*, vol. 103, p. 102718, 2021.

[28] Z. Liu, Y. Xu, Y. Lin, et al., "High-Q quasibound states in the continuum for nonlinear metasurfaces," *Phys. Rev. Lett.*, vol. 123, p. 253901, 2019.

[29] S. Joseph, S. Pandey, S. Sarkar, and J. Joseph, "Bound states in the continuum in resonant nanostructures: an overview of engineered materials for tailored applications," *Nanophotonics*, vol. 10, pp. 4175−4207, 2021.

[30] A. Kodigala, T. Lepetit, Q. Gu, et al., "Lasing action from photonic bound states in continuum," *Nature*, vol. 541, pp. 196−199, 2017.

[31] D. C. Marinica, A. G. Borisov, and S. V. Shabanov, "Bound states in the continuum in photonics," *Phys. Rev. Lett.*, vol. 100, p. 183902, 2008.

[32] Y. Yang, C. Peng, Y. Liang, Z. Li, and S. Noda, "Analytical perspective for bound states in the continuum in photonic crystal slabs," *Phys. Rev. Lett.*, vol. 113, p. 037401, 2014.

[33] K. Koshelev, Y. Tang, K. Li, et al., "Nonlinear metasurfaces governed by bound states in the continuum," *ACS Photonics*, vol. 6, pp. 1639−1644, 2019.

[34] P. Facchi, D. Lonigro, S. Pascazio, F. V. Pepe, and D. Pomarico, "Bound states in the continuum for an array of quantum emitters," *Phys. Rev. A*, vol. 100, p. 023834, 2019.

[35] P. T. Fong and C. K. Law, "Bound state in the continuum by spatially separated ensembles of atoms in a coupled-cavity array," *Phys. Rev. A*, vol. 96, p. 023842, 2017.

[36] G. Calajó, Y. L. Fang, H. U. Baranger, and F. Ciccarello, "Exciting a bound state in the continuum through multiphoton scattering plus delayed quantum feedback," *Phys. Rev. Lett.*, vol. 122, p. 073601, 2019.

[37] C. Sauvan, J. P. Hugonin, I. S. Maksymov, and P. Lalanne, "Theory of the spontaneous optical emission of nanosize photonic and plasmon resonators," *Phys. Rev. Lett.*, vol. 110, p. 237401, 2013.

[38] S. Hughes, M. Richter, and A. Knorr, "Quantized pseudomodes for plasmonic cavity QED," *Opt. Lett.*, vol. 43, pp. 1834−1837, 2018.

[39] R. J. Brecha, P. R. Rice, and M. Xiao, "N two-level atoms in a driven optical cavity: quantum dynamics of forward photon scattering for weak incident fields," *Phys. Rev. A*, vol. 59, pp. 2392−2417, 1999.

[40] D. Tamascelli, A. Smirne, S. F. Huelga, and M. B. Plenio, "Nonperturbative treatment of non-markovian dynamics of open quantum systems," *Phys. Rev. Lett.*, vol. 120, p. 030402, 2018.

[41] E. V. Denning, J. Iles-Smith, and J. Mork, "Quantum light-matter interaction and controlled phonon scattering in a photonic fano cavity," *Phys. Rev. B*, vol. 100, p. 214306, 2019.

[42] E. Z. Casalengua, J. C. López Carreño, F. P. Laussy, and E. D. Valle, "Conventional and unconventional photon statistics," *Laser Photon. Rev.*, vol. 14, p. 1900279, 2020.

[43] E. Z. Casalengua, J. C. López Carreño, F. P. Laussy, and E. del Valle, "Tuning photon statistics with coherent fields," *Phys. Rev. A*, vol. 101, p. 063824, 2020.

[44] H. J. Snijders, J. A. Frey, J. Norman, et al., "Observation of the unconventional photon blockade," *Phys. Rev. Lett.*, vol. 121, p. 043601, 2018.

[45] R. Horodecki, P. Horodecki, M. Horodecki, and K. Horodecki, "Quantum entanglement," *Rev. Mod. Phys.*, vol. 81, pp. 865−942, 2009.

[46] W. K. Wootters, "Entanglement of formation of an arbitrary state of two qubits," *Phys. Rev. Lett.*, vol. 80, pp. 2245−2248, 1998.

[47] J. R. Johansson, P. D. Nation, and F. Nori, "QuTiP 2: a Python framework for the dynamics of open quantum systems," *Comput. Phys. Commun.*, vol. 184, pp. 1234−1240, 2013.

[48] W. K. Mok, J. B. You, L. C. Kwek, and D. Aghamalyan, "Microresonators enhancing long-distance dynamical entanglement generation in chiral quantum networks," *Phys. Rev. A*, vol. 101, p. 053861, 2020.

[49] J. Hakami and M. S. Zubairy, "Nanoshell-mediated robust entanglement between coupled quantum dots," *Phys. Rev. A*, vol. 93, p. 022320, 2016.

[50] S. Nicolosi, A. Napoli, A. Messina, and F. Petruccione, "Dissipation-induced stationary entanglement in dipole-dipole interacting atomic samples," *Phys. Rev. A*, vol. 70, p. 022511, 2004.

[51] A. C. Downing, D. Zueco, and L. Martín-Moreno, "Chiral current circulation and PT symmetry in a trimer of oscillators," *ACS Photonics*, vol. 7, pp. 3401−3414, 2020.

[52] P. Roushan, C. Neill, A. Megrant, et al., "Chiral ground-state currents of interacting photons in a synthetic magnetic field," *Nat. Phys.*, vol. 13, pp. 146−151, 2017.

[53] M. Yamaguchi, A. Lyasota, and T. Yuge, "Theory of Fano effect in cavity quantum electrodynamics," *Phys. Rev. Research*, vol. 3, p. 013037, 2021.

[54] K. As'ham, I. Al-Ani, L. Huang, A. E. Miroshnichenko, and H. T. Hattori, "Boosting strong coupling in a hybrid WSe2 monolayer−anapole−plasmon system," *ACS Photonics*, vol. 8, pp. 489−496, 2021.

[55] R. Verre, D. G. Baranov, B. Munkhbat, et al., "Transition metal dichalcogenide nanodisks as high-index dielectric Mie nanoresonators," *Nat. Nanotechnol.*, vol. 14, pp. 679−683, 2019.

[56] Q. Zhao, W. J. Zhou, Y. H. Deng, et al., "Plexcitonic strong coupling: unique features, applications, and challenges," *J. Phys. D*, vol. 55, p. 203002, 2022.